# Nonlinear Strain Stiffening Is Not Sufficient to Explain How Far Cells Can Feel on Fibrous Protein Gels

Mathilda S. Rudnicki,[†] Heather A. Cirka,[†] Maziar Aghvami,[§] Edward A. Sander,[§] Qi Wen,[‡] and Kristen L. Billiar[†*]
[†]Department of Biomedical Engineering and [‡]Department of Physics, Worcester Polytechnic Institute, Worcester, Massachusetts; and [§]Department of Biomedical Engineering, University of Iowa, Iowa City, Iowa

ABSTRACT Recent observations suggest that cells on fibrous extracellular matrix materials sense mechanical signals over much larger distances than they do on linearly elastic synthetic materials. In this work, we systematically investigate the distance fibroblasts can sense a rigid boundary through fibrous gels by quantifying the spread areas of human lung fibroblasts and 3T3 fibroblasts cultured on sloped collagen and fibrin gels. The cell areas gradually decrease as gel thickness increases from 0 to 150 $\mu$m, with characteristic sensing distances of >65 $\mu$m below fibrin and collagen gels, and spreading affected on gels as thick as 150 $\mu$m. These results demonstrate that fibroblasts sense deeper into collagen and fibrin gels than they do into polyacrylamide gels, with the latter exhibiting characteristic sensing distances of <5 $\mu$m. We apply finite-element analysis to explore the role of strain stiffening, a characteristic mechanical property of collagen and fibrin that is not observed in polyacrylamide, in facilitating mechanosensing over long distances. Our analysis shows that the effective stiffness of both linear and nonlinear materials sharply increases once the thickness is reduced below 5 $\mu$m, with only a slight enhancement in sensitivity to depth for the nonlinear material at very low thickness and high applied traction. Multiscale simulations with a simplified geometry predict changes in fiber alignment deep into the gel and a large increase in effective stiffness with a decrease in substrate thickness that is not predicted by nonlinear elasticity. These results suggest that the observed cell-spreading response to gel thickness is not explained by the nonlinear strain-stiffening behavior of the material alone and is likely due to the fibrous nature of the proteins.

## INTRODUCTION

The mechanical environment of a cell regulates its behavior and in doing so influences processes on a larger scale, such as tissue development and disease progression. These affected behaviors include differentiation, morphology, and spreading (1–3). Although important aspects of mechanosensing have been revealed, such as the role played by cell-generated tension (4–6), many details of mechanotransduction have yet to be elucidated.

Fundamental to understanding how a cell senses its environment and interacts mechanically with other cells and structures is the question of how far a cell can feel. Both computer modeling and experimental observations have demonstrated that cells are able to sense mechanical signals beyond their physical boundaries. Discher and colleagues (7) modeled the strain field between contracting cells on linear elastic substrates using finite-element analysis (FEA) and concluded that human mesenchymal stem cells (hMSCs) can sense nearby cells that are within one cell length apart (<40 $\mu$m). Experimental results of increased spreading area of hMSCs and fibroblasts on low-stiffness (1 kPa) polyacrylamide (PA) gels with decreased substrate thicknesses (8–10) are consistent with the aforementioned FEA results. Cell spread area is considered a sensitive indicator of the degree to which the cell can sense the underlying rigid substrate, as spreading is known to increase with substrate stiffness (9,11–13). Reinhart-King (14) reported a similar lateral distance of mechanical transmission (~30 $\mu$m) for bovine aortic endothelial cells based on traction force microscopy measurements and cell-generated bead displacements 30–50 $\mu$m from the edge of cells cultured on intermediate-stiffness PA gels (2–5.5 kPa). In contrast to results for PA gels, Winer et al. (15) found that hMSCs and 3T3 fibroblasts on fibrin gels can significantly deform the gel up to five cell lengths away. Long-distance mechanosensing was also shown by Leong et al. (16), who reported a greater hMSC spread area on 130-$\mu$m-thick soft collagen gels than on 1440-$\mu$m-thick gels (8). Although it is becoming clear that cells are able to sense substantially farther both laterally and in depth on fibrin and collagen gels than on PA gels, the mechanism by which mechanical signals are propagated through protein gels is not known.

Three major differences exist between protein and synthetic gels that may explain the differences in transmission of mechanical signals. Whereas PA gels consist of polymers of small chain diameter and length relative to the scale of a cell and are linear elastic over a wide range of frequencies and strains, protein gels are viscoelastic, are fibrous in nature, and exhibit nonlinear behavior (i.e., they are strain-stiffening materials) (17). Substrate viscoelasticity, whether due to the biphasic (solid/fluid) nature of the gels or the intrinsic viscoelasticity of the fibers (18), decreases the ability of a cell to transmit mechanical signals through the matrix. Stress signals generated by cell-generated displacements relax with time, and substrate creep has been shown to reduce isometric cytoskeletal tension in mesenchymal stem cells (19). In contrast, fibers may extend

*Submitted November 28, 2012, and accepted for publication May 10, 2013.*

*Correspondence: kbilliar@wpi.edu

Editor: Alissa Weaver.



0006-3495/13/07/0011/10 $2.00

http://dx.doi.org/10.1016/j.bpj.2013.05.032

stress transmission, because cell-generated traction forces may propagate preferentially along relatively stiff fibers. The strain-stiffening property of protein gels has also been hypothesized to facilitate long-distance mechanical communication between cells (15).

Our goal in this work was to characterize depth sensing of fibroblasts on protein gels and to test the hypothesis that cells can sense farther into fibrin and collagen gels than into linear materials due to the strain-stiffening material property of the protein gels. We systematically investigated fibroblast spreading on fibrin and collagen gels of variable thickness, and quantified the relationship between spread area and substrate thickness to determine the characteristic sensing distance of cells on protein gels. Because currently it is not experimentally feasible to separate strain-stiffening behavior from the fibrous nature of protein gels, we used finite-element (FE) models to numerically simulate cells by applying traction to substrates of different thicknesses and intrinsic properties, including fibrous and nonfibrous nonlinear gel models. We quantitatively analyzed the results to determine whether strain-stiffening behavior and/or fiber mechanics can explain how far cells can feel on fibrous protein gels.

## MATERIALS AND METHODS

### Experimental studies

#### *Gel mold design and sample preparation*

Rather than creating multiple gels of different thickness, we developed a novel (to our knowledge) sloped-gel method to study cell behavior as a function of substrate thickness within the same sample. We created wedge-shaped gels by polymerizing gels between two glass slides with a spacer on one side, as shown in Fig. 1 *A*. To create a wedge shape, the substrate must firmly attach to the bottom glass piece, yet separate easily from the top culture surface. The lower slide to which the gel should adhere firmly was activated as described by Pelham and Wang (20). The top glass slide was left untreated because antiadhesion coatings (Rain-X, Houston, TX) and Sigmacote (Sigma-Aldrich, St. Louis, MO) were observed to affect the health of the cells. We used two No. 1 coverslips (18 × 18 mm × 150 $\mu$m; Electron Microscopy Sciences, Hatfield, PA) as spacers between the two glass slides by attaching the coverslips to the bottom slide with medical-grade silicone adhesive (Blue Star Silicones, Hoboken, NJ).

We prepared fibrin gels at room temperature by polymerizing fibrinogen and thrombin (Sigma-Aldrich) with calcium as described by Balestrini et al. (21), which resulted in a cross-linked network structure. Briefly, a mixture of fibrinogen, Dulbecco's modified Eagle's medium (DMEM; Invitrogen, Grand Island, NY), and calcium was added to a mixture of thrombin and HBSS (20 mM HEPES in 0.9% NaCl saline solution) to bring the fibrinogen concentration to 4.5 mg/mL. After 15 min, the top glass slide was removed and the gel was allowed to polymerize for an additional 45 min in DMEM. Collagen gels were prepared with a solution of acid-extracted rat-tail tendon collagen mixed with concentrated DMEM to achieve a final collagen concentration of 4 mg/mL at 4°C to minimize polymerization during sample preparation. The gels were polymerized between the sloped glass slides after neutralization with sodium hydroxide at room temperature for ~1 h. The schematics of a finished sample ready for use, dry, and submerged in media are shown in Fig. 1, *B* and *C*, respectively.

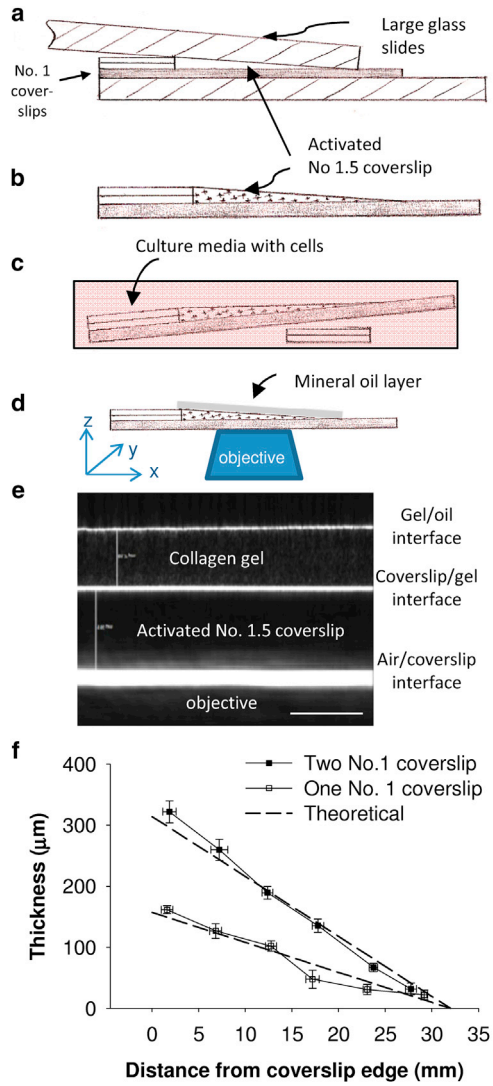


FIGURE 1 (*a*) Schematic of the experimental setup for creating the sloped-gel sample. The collagen or fibrin gel adheres to the activated No. 1.5 coverslip and is formed into the sloped shape by the upper large glass slide that is weighted with a 50 g object. (*b*) Schematic of the finished sample ready for cell seeding. (*c*) Samples are placed in a 100 mm petri dish and the right side is propped up with two No. 1 coverslips to ensure a level seeding surface. (*d*) Sample setup for imaging with mineral oil to minimize reflection at the edge of the gel. (*e*) Confocal reflectance image taken in cross-section mode shows the No. 1.5 coverslip between the bottom and middle white lines, and protein gel fibers with speckled pattern between the top two lines (10× dry objective; scale bar = 100 $\mu$m). The change in height (~4 $\mu$m) cannot be readily seen over the field of view (~400 $\mu$m) due to the gradual slope of the gel. (*f*) Validation of the slopes of fibrin gels created in the system using either one or two No. 1 coverslips.

#### *Cell culture*

Human lung fibroblasts (HLFs, P5–P7) and 3T3-J2 fibroblasts (3T3, P7), graciously donated by Prof. George Pins (Worcester Polytechnic Institute), were cultured in DMEM with 1% streptomycin/penicillin and 10% fetal bovine serum for HLFs or 10% bovine calf serum for 3T3s, and incubated at 10% $CO_2$. Samples were seeded at ~3000 cells/cm$^2$. To ensure a level substrate for the cells, the end of the sample with the thinner side of the substrate was propped up by the appropriate amount (Fig. 1 *C*). To make sure

the cell suspension remained atop the gel, rectangular frames cut from a thin silicone sheet (0.015"; Specialty Manufacturing, Inc., Saginaw, MI) were placed on the gel immediately before cell seeding and then removed after seeding. Cells were cultured overnight (~16 h) and then processed for imaging. HLFs and 3T3s were each cultured on collagen gels, and HLFs were also cultured on fibrin gels.

### *Imaging for cell area and gel thickness*

Before imaging, the gels and cells were fixed with 4% paraformaldehyde for 15 min. After two 5-min rinses with PBS, the cells were stained for F-actin with phalloidin (488; Invitrogen) and incubated for 30 min at 37°C. After three 10-min rinses, the nuclei were stained with Hoechst 33342 (Invitrogen) for 3–5 min and rinsed twice with PBS.

To determine the thickness of the gel beneath the cells, an inverted confocal microscope (TCS SP5; Leica Microsystems GmbH, Wetzlar, Germany) with a 10× objective was used in reflectance mode. Rather than measuring thickness from reconstructed z-stacks in the standard imaging mode (XYZ), we utilized cross-section (XZY) imaging mode, yielding images as shown in Fig. 1 *E*. The bright lines are the result of differences in refractive index between the materials: the lower line is between air and glass, the next line is between the glass and collagen gel, and the top line indicates the gel/mineral-oil interface. The network of the protein gel can be seen as a speckled pattern. Due to the ratio of refractive indices of glass and air, the ratio of the true micrometer-measured distances and the image-measured distances is 1.5. This ratio was used to correct the confocal image-based gel thickness measurements. The slopes of the gels were verified by thickness measurements from confocal reflectance images taken along the length of the gel (Fig. 1 *F*).

We imaged FITC phalloidin-labeled cells using a Leica inverted confocal microscope with a 10× objective in fluorescence mode. We quantified the cell areas from the confocal images using the Analyze Particles tool of ImageJ (rsb.info.nih.gov/ij/) and custom MATLAB code (The MathWorks, Natick, MA). We first thresholded the images to highlight the cells, and then visually compared them with the original image to ensure that the threshold level was acceptable. Upon review of the images, areas that contained only one nucleus and were at least 50 $\mu$m away from the nearest cell were included in the quantification. In addition, the tool was set to exclude thresholded areas along the edges of the image and to include holes within closed loops.

### *Quantification of the relationship between cell-spread area and substrate thickness*

To quantify the relationship between cell-spread area, $A$, and substrate thickness, $h$, we fit the data to a three-parameter rational equation using SigmaPlot (Systat Software, Inc., San Jose, CA):

$$A(h) = \frac{a}{1 + h/h_{50}} + A_\infty . \tag{1}$$

The parameter $a$ is a scaling factor in units of area; larger cell types have higher $a$-values than those that spread more moderately. $A_\infty$ represents the spread area of a cell on a gel of infinite thickness. The parameter $h_{50}$ represents the substrate thickness at which the curve reaches 50% of the maximal value over the baseline value, i.e., the spread area of cells on gels of this thickness on average is halfway between that of cells on an infinitely thick gel and cells on an infinitely thin (rigid) substrate.

### *Assessment of cell reorganization of fibrous structure*

The extent of fiber reorganization near cells was quantified along the surface and into the depth of collagen and fibrin gels. Intensity profiles from the cells outward along 100 pixel-wide analysis regions (intensity averaged over width) were determined using ImageJ, and the distance from the edge of the cell where the intensity decayed to the background value was calculated by curve fitting in MATLAB (Fig. S1 in the Supporting Material). To quantify how deeply into the gel the fiber patterns were disturbed due to cell-mediated remodeling, we analyzed 16-bit grayscale intensity histograms of successive z-stack images spaced at 0.5 $\mu$m for the degree of normality of the data. Skewing of an intensity distribution was considered significant (nonGaussian) if the normal probability plot was linear for <80% of the data (Fig. S2; see Supporting Material for analysis details).

## FE models

### *Linear and nonlinear elastic material models*

A radially symmetric FE model of a cell exerting inward traction on the surface of a finite-thickness gel was developed based on Sen et al. (7), with cell-gel interface conditions based on Mehrotra et al. (22) and Munevar et al. (23). A constant traction along the focal adhesion area of width $A$ (8.6 $\mu$m) was applied at a mean radius $R$ (13.4 $\mu$m) from the axis of symmetry (Fig. S3). Six-node-modified quadratic axisymmetric triangular (CAX6M) elements were utilized, and elements ranged in number from 200 (for 0.3 $\mu$m thickness) to 8000 (for 50 $\mu$m thickness) per simulation in ABAQUS (v. 6.8; ABAQUS, Providence, RI). Elastic moduli of 0.6–40 kPa were utilized with a Poisson ratio of 0.49.

To investigate the effect of material strain stiffening on propagation of stress and strain in the substrate, we input published nonlinear mechanical properties of a 2 mg/mL fibrin gel (15) over a range of 2–100% shear strain into the FE model (see stress-strain curve in Fig. S4 *A*). Material models with more pronounced strain stiffening behavior were also utilized (Fig. S4, *B* and *C*). To quantify the relationship between maximum surface displacement, $u_{max}$, and substrate thickness, $h$, we fit the simulated data to a hyperbolic equation per Sen et al. (7):

$$u_{max} = \frac{u_{inf} * h}{h + h_{crit}} \tag{2}$$

where $u_{inf}$ is the saturation displacement on a semi-infinite substrate, and $h_{crit}$ is a parameter indicating the substrate thickness corresponding to half-maximal displacement. Whereas $u_{max}$ decreases with increasing substrate stiffness, $h_{crit}$ is the same for all linear substrates in our FE model due to the linearity of the solution.

We compared the responses of substrates of different thicknesses and intrinsic properties quantitatively by calculating the effective stiffness, $E_{eff}$, adapted from Mehrotra et al. (22):

$$E_{eff} = C\frac{T}{u_{max}/\overline{R}} \tag{3}$$

where $T$ is the radially applied traction, $\overline{R}$ is the mean radius of the focal adhesion area, and $C$ is a scaling factor that equates $E_{eff}$ to the Young's modulus of an infinitely thick linear gel for a given set of geometric factors ($R$ and $A$). For the chosen annular traction region in our FE model, $C = 1.7$, such that $E_{eff} = E_{gel}$ for a 50-$\mu$m-thick linear gel. Unlike the surface displacements, $E_{eff}$ is independent of the magnitude of traction applied to a linear gel.

### *Nonlinear fibrous model*

To investigate the role of protein fibers in the propagation of stress in a fibrous substrate, we adapted a multiscale fiber-based FE model to the problem (for details, see Stylianopoulos and Barocas (24) and Sander et al. (25)). The model consists of an FE domain and a collection of microscopic fiber networks. FE domains (one element wide (4 $\mu$m), 25 elements long (75 $\mu$m), and 200, 600, or 1000 elements thick (10 $\mu$m, 30 $\mu$m, and 50 $\mu$m, respectively)) with trilinear hexahedral elements were created as simplified rectangular versions of the full radially symmetric FE model geometry described above. Two hundred unique and nominally isotropic fiber networks were created and randomly associated with an element in

the model. The material properties of the fibers were selected to match the bulk material nonlinearity of a fibrin gel (15) or a collagen gel (25). Fixed boundary conditions were applied to the bottom and right faces, and symmetry boundary conditions were applied to the left, front, and back faces. The nodes on the upper surface were free, except for those in the focal adhesion area (8.6 $\mu$m long and 4 $\mu$m wide) at a mean distance of 13.4 $\mu$m from the left boundary (matching the region where traction is applied in our standard model; Fig. S3 *C*). The nodes associated with the focal adhesion area were displaced 2.5 $\mu$m inward (to the left), and the resulting stress field was computed. For direct comparison, a nonlinear continuum model of the same material properties, geometry, loading, and boundary conditions was created in ABAQUS as described above.

## RESULTS

### Experimental results

#### *Cell-spread area is highly dependent upon gel thickness*

The cells attached and spread on the surface of the fibrin and collagen gels, with the final spread area dependent upon cell type and location along the sloped gels corresponding to thickness. We quantified cell spreading for cells cultured on sloped collagen gels, and measured the thickness below each cell using confocal reflectance cross-sectional imaging. Representative images show the difference in spread area of HLFs on thick (Fig. 2 *A*) and thin (Fig. 2 *B*) fibrin gels. The cell-spread areas span from 500 to 7000 $\mu m^2$, with HLFs being larger than 3T3 fibroblasts and more spread on collagen than on fibrin. Although alignment was not quantified in this study, there did not appear to be any obvious preferred alignment direction for the cells. Representative overlays of confocal fluorescence images of lung fibroblasts on confocal reflection images of underlying fibrin (Fig. 2 *C*) and collagen (Fig. 2 *D*) gels show the substantial interaction between the cells and the proteins during culture.

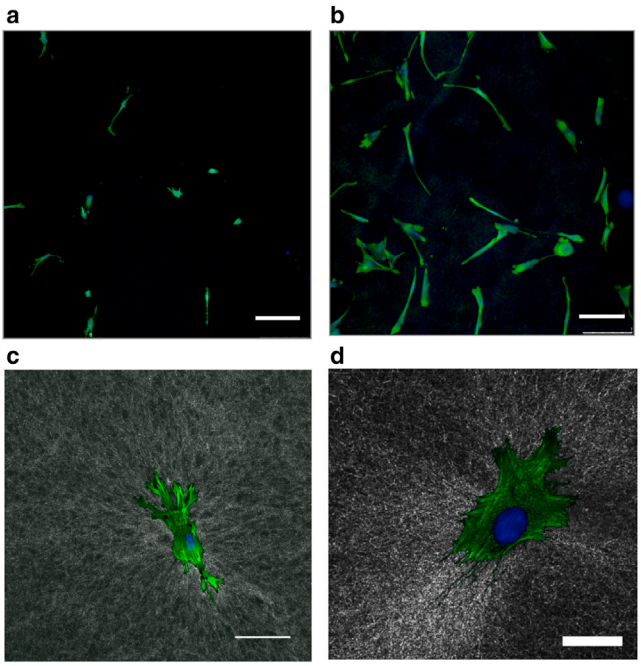


FIGURE 2 Representative fluorescent micrographs of HLFs on thick (*a*) and thin (*b*) fibrin gels used for cell area analysis (10× dry objective; scale bars = 250 $\mu$m). Actin cytoskeleton stained with phalloidin (*green* in color, *light grey* in greyscale) and nuclei stained with Hoescht (*blue* in color, *dark grey* in greyscale) after 16 h culture period. Confocal reflectance images (in standard XYZ mode) of fibrin (*c*) and collagen (*d*) gels with fluorescent stain overlays reveal local reorganization by cells, indicating stress/strain propagation through the fibrous network. (*c*) 20× oil objective; scale bar = 75 $\mu$m; (*d*) 40× oil objective; scale bar = 25 $\mu$m.

Cell areas for various positions every 5 mm along the sloped gels are shown in Fig. 3. For the thinnest gel regions that could be reliably quantified (~20 $\mu$m), the cell-spread area was approximately the same as on the coverslip beyond the sloped gel (*solid symbols* at zero thickness in Fig. 3) and on the rigid control surfaces (*open symbols* in Fig. 3). All cell types gradually decreased in area as the gel thickness increased for both collagen and fibrin substrates. Equilibrium (minimum) area values did not appear to be reached on the thickest region that could be imaged by our equipment (150 $\mu$m), indicating that the cells can transmit mechanical signals farther than this depth in protein gels. To obtain a more robust $A_\infty$ value, we also cultured 3T3 cells on a separate 1-mm-thick gel.

To quantitatively assess the relationship between cell area and substrate thickness, we fit our data for the cells on protein gels and values from the literature for cells on PA gels to Eq. 1 (see Table 1 for fit parameters). The relatively large values of $h_{50}$ for the cells cultured on protein gels (67–94 $\mu$m) indicate a gradual spreading response to nonlinear

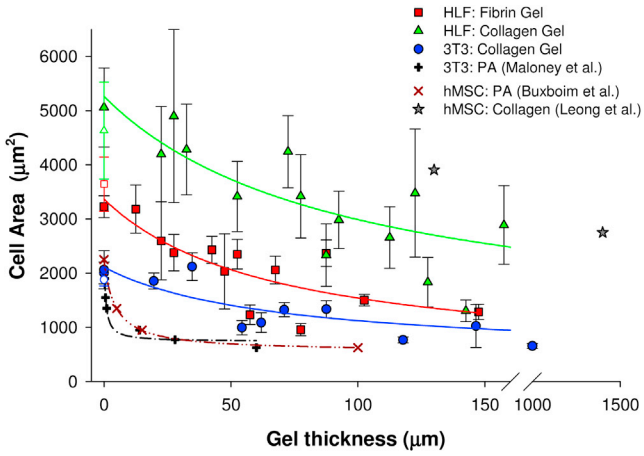


FIGURE 3 Cell spreading as a function of gel thickness for HLFs on fibrin (*red squares*) and collagen (*green triangles*) gels, and for 3T3s on fibrin gels (*blue circles*). Reported as mean ± SE; HLFs on collagen, mean = 9 cells per data point, $n = 4$ gels; HLFs on fibrin, mean = 10 cells per data point, $n = 5$ gels; 3T3 on collagen, mean = 20 cells per data point, $n = 2$ gels. Open symbols indicate control cells on tissue culture plastic. Data from the literature for 3T3 fibroblasts (+ symbols) and hMSCs (x symbols) indicate that cells on PA gels are not affected by rigid boundaries more than ~30 $\mu$m away. On nonlinear fibrin and collagen gels, fibroblasts sense the rigid boundary on much thicker gels (>100 $\mu$m), consistent with the spread area of hMSCs on collagen gels (star symbols), and the relationship between spread area and thickness is more gradual than on PA gels.

**TABLE 1 Parameter values for rational fit of cell area versus gel thickness ($A(h) = a/(1 + h/h_{50}) + A_\infty$)**

| Cell type | Substrate | $a$ ($\mu m^2$) | $h_{50}$ ($\mu$m) | $A_\infty$ ($\mu m^2$) | $r^2$ | Reference |
|---|---|---|---|---|---|---|
| HLF | 4.5 mg/ml fibrin | 3060 | 67 | 313 | 0.67 | |
| HLF | 4 mg/ml collagen | 4420 | 94 | 842 | 0.61 | |
| 3T3 | 4 mg/ml collagen | 1660 | 68 | 455 | 0.77 | |
| 3T3 | 1 kPa PA | 1710 | 0.61 | 737 | 0.97 | (9) |
| hMSC | 5.6 kPa PA | 1690 | 4.5 | 556 | 0.99 | (8) |

The higher values of $h_{50}$ on protein gels indicate a greater sensing depth on these gels than on linear PA gels.

fibrous substrates of decreasing thickness and a much larger sensing distance compared with those on PA gels, which had low $h_{50}$ values (0.6–4.5 $\mu$m).

*Cells reorganize the surrounding fibrous network*

Analyses of confocal reflectance image intensity profiles indicate that the fibrous structures of the gels were substantially reorganized a minimum of 20 $\mu$m and up to 200 $\mu$m from the edge of a cell along the surface of the gels (Fig. S1). Measureable alterations of the fibrous structure were observed 7–8.5 $\mu$m into the depth of the collagen gel beneath the cell (Fig. S2). Because removal of the cells from nonfixed gels with trypsin disrupted the gel structure, we could not determine whether the dense areas emanating from the cells represent active cell-generated tension in the matrix or permanent remodeling.

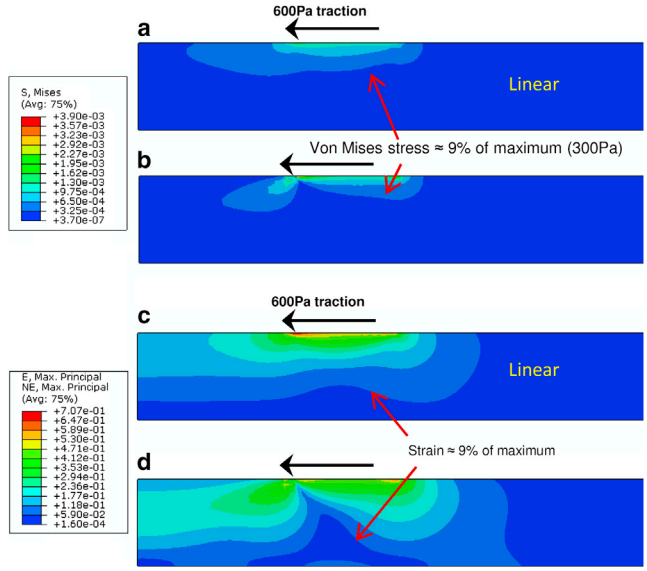


FIGURE 4 (*a–d*) Stress (*a* and *b*; in MPa) and strain (*c* and *d*; unitless) distributions for 2 kPa linear (*a* and *c*) and nonlinear (*b* and *d*) gels of 10 $\mu$m thickness with 600 Pa traction applied. Plots for the other stiffness linear gels have different magnitude but when normalized to maximum values look identical (data not shown). The stress contours are blunted and exhibit a pinched profile in the strain-stiffening material. In contrast, the strain profiles extend farther into the strain-stiffening material compared with the linear material, as can be seen by the lowest contour, representing roughly 9% of the maximum strain, touching the lower boundary in the 10-$\mu$m-thick nonlinear gel but not in the 10-$\mu$m-thick linear gel. See Supporting Material for plots for 1, 5, and 50 $\mu$m gels.

## FE simulations

*Strain-stiffening behavior blunts stress contours and extends strain contours*

The stress and strain contour plots for linear (2 kPa) and nonlinear gels of 10 $\mu$m thickness with 600 Pa of applied traction are shown in Fig. 4. The magnitudes of the stresses are similar for the linear and nonlinear materials (~4 kPa maximum von Mises stress), yet the form of the stress field is altered in the strain-stiffening material. The extent of the stress contours is blunted compared with the linear material and there is a pinched pattern at the inner edge of the annulus where traction is applied and the stress is maximal. We confirmed that the pinched pattern was not a computational artifact by remeshing the material with both triangle and quadrilateral elements where each produced identical patterns (data not shown). The strain profiles extend further into the strain-stiffening material than into the linear material, as can be seen by the lowest contour, representing roughly 9% of the maximum strain, touching the lower boundary in the 10-$\mu$m-thick nonlinear gel (Fig. 4 *D*), but not in the linear gel (Fig. 4 *C*).

Surface displacement values normalized to the results for the thickest gel match the displacement-thickness relationship computed by Sen et al. (7) (Fig. S5). Stress contour plots for different levels of traction are shown in Fig. S6 and peak displacements as a function of traction are given in Fig. S7. The effect of the location of application of traction on the surface is plotted in Fig. S8. Stress and strain contour plots for 1, 10, and 50 $\mu$m gel thickness with 600 Pa of applied traction are provided in Figs. S9 and S10, respectively; those for 0.3, 2.5, 5, 12, 15, and 20 $\mu$m look similar and are not shown due to space constraints. The magnitude of strain scales inversely with the material modulus, but the depth and lateral extent to which the normalized contours extend are the same for all linear materials, and thus results for only the 2 kPa gel are shown. The maximum surface displacement values for all gel thickness values and stiffness levels are provided in Table S1.

*Maximum substrate displacement is lower on thinner gels*

For a given level of traction, the maximum predicted displacement is lower for thin than for thick linear elastic gels due to proximity of the rigid lower boundary. The largest differences occur between 0 and 10 $\mu$m. The response saturates (negligible increase in displacement) for substrates $>$ 50 $\mu$m thick (Fig. 5 *A*). The dependence of the displacement on the gel thickness is similar for the strain-stiffening material. Despite having an initial modulus of well below 1 kPa, the strain-stiffening material behaves similarly to a 2 kPa gel with a 600 Pa traction force applied (Fig. 5 *A*). A more nonlinear material with the same low

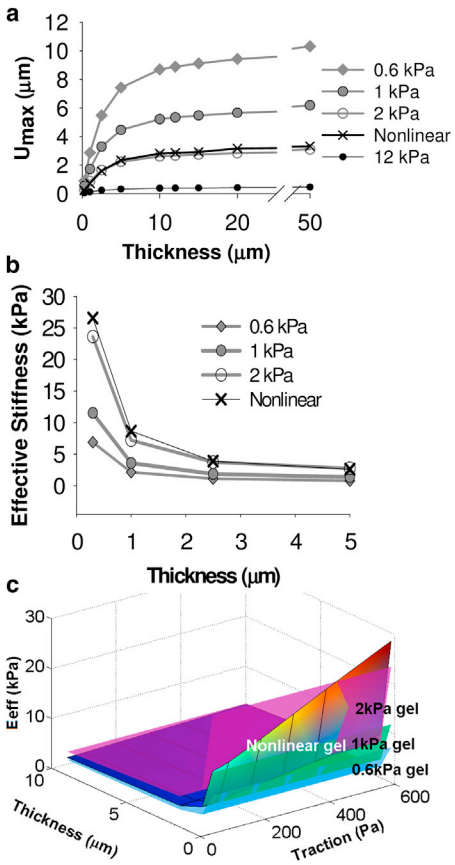


FIGURE 5 (*a*) For a given applied traction (600 Pa), substrate displacement decreases with decreasing thickness and increasing gel stiffness. (*b*) The strain-stiffening behavior causes the nonlinear material to become effectively stiffer at low thicknesses ($h < 2$ $\mu$m) when the applied traction is increased. (*c*) A surface plot of effective stiffness as a function of applied traction (100–600 Pa) and thickness (0.5–10 $\mu$m) shows that the nonlinear material (*gradient colored*) exhibits an effective stiffness similar to that of the 1 kPa linear material with 100 Pa applied traction, but is more stiff than the 2 kPa linear material with tractions over ~500 Pa at low thicknesses. When viewed in greyscale, darker colors indicate lower values except immediately under the loading at the upper surface.

modulus (at 10% strain) and high modulus (at 80% strain), but with stiffening occurring at higher strain values and greater curvature, was also utilized (Fig. S4 *B*). Similar relationships between displacement and thickness were found regardless of the degree of nonlinearity (e.g., little relative change in displacement for substrates $> 10$ $\mu$m; Fig. S4 *C*).

For a quantitative comparison of the response on the different substrates, the $u_{max}$ and thickness data were fit to a hyperbolic equation (Eq. 2); parameter values are listed in Table 2. The maximum surface displacement that occurs when a cell applies a given traction may provide an indication of the stiffness that the cell feels. By inverting Eq. 3, we can calculate the thickness that yields a given displacement at an applied traction level. This analysis suggests that a cell on a 0.05-$\mu$m-thick 1 kPa gel would deflect the surface the same amount (0.1 $\mu$m) as a cell on a 13-$\mu$m-thick 40 kPa gel (see Table 2), i.e., these two substrates would have the same

**TABLE 2 Fit parameters for a hyperbolic relationship ($u = u_{inf}\, h/(h + h_{crit})$) for the FE data in Fig. 5 *A* and calculated thickness, $h$(0.01 $\mu$m), corresponding to a maximum surface displacement of 0.1 $\mu$m**

| FE model | $E$ (kPa) | Applied traction (Pa) | $u_{inf}$ ($\mu$m) | $h_{crit}$ ($\mu$m) | $h$ (0.1 $\mu$m) |
|---|---|---|---|---|---|
| Linear | 1 | 400 | 4.72 | 2.41 | 0.052 |
| | 5 | 400 | 0.94 | 2.41 | 0.29 |
| | 12 | 400 | 0.39 | 2.41 | 0.82 |
| | 40 | 400 | 0.12 | 2.41 | 13.3 |
| Nonlinear | | 400 | 2.90 | 3.26 | 0.12 |
| | | 600 | 3.61 | 3.19 | 0.09 |

effective stiffness to the cell. The calculated effective stiffness values (Eq. 3) decrease rapidly from 0 to 2.5 $\mu$m thickness, and saturate to a value close to the bulk stiffness for substrates thicker than 5 $\mu$m (Fig. 5 *B*). The nonlinear material behaves similarly to the 2 kPa gel down to 2.5 $\mu$m thickness, and has a slightly higher effective stiffness for substrates <2.5 $\mu$m thick. The effects of both applied traction level and thickness on effective stiffness are shown as a surface plot in Fig. 5 *C*, where it can be observed that the nonlinear gel becomes effectively stiffer than the 2 kPa linear gel for $T > 400$ Pa and $t < 2.5$ $\mu$m.

### *Effective stiffness is more sensitive to gel thickness for the fibrous model*

The propagation of stress (Fig. 6 *A*) and strain (Fig. 6 *B*) through the fibrous model is qualitatively and quantitatively different from that observed for the nonlinear continuum model. The simulated fiber population, which is initially uniform, reorients toward the displaced region on the surface, and a substantial change in the degree of fiber alignment is observed through the depth of the 10 $\mu$m model (Fig. 6 *C*) and extends >20 $\mu$m through the gel (Fig. 6 *C*, *inset*). The predicted fiber network realignment was somewhat less extensive in the 30 and 50 $\mu$m models (Fig. S11). Despite exhibiting the same bulk tensile stress-strain behavior, the magnitudes of stress in the multiscale model are two- to fourfold lower than observed for the continuum model. Addition of an isotropic incompressible matrix supporting the fibers would likely increase the stress in the model to the level of the continuum model. For direct comparison, the results of each model are presented relative to the output for the thickest model of each type. The normalized analysis reveals that the dependence of effective stiffness on thickness is more pronounced for the fibrous models than for the continuum nonlinear model. Relative to the 50-$\mu$m-thick model, the effective stiffness of the 30-$\mu$m-thick model is 50% higher in the fibrous fibrin model but only 2% higher in the continuum model. For the 10-$\mu$m-thick model, the effective stiffness values are 125% and 29% higher than the 50-$\mu$m-thick model for the fibrous fibrin and continuum models, respectively (Fig. 6 *D*). The use of parameters matching those of a collagen gel had a less pronounced effect on the effective stiffness-thickness

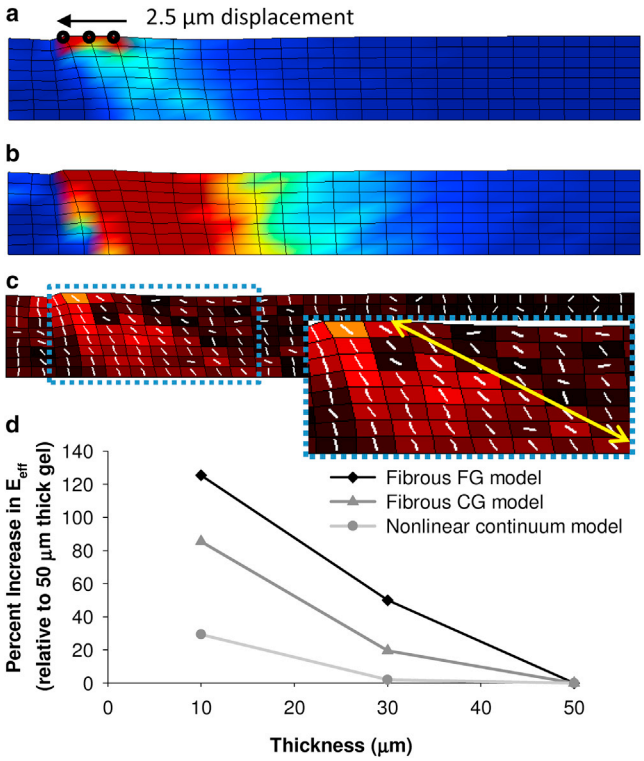


FIGURE 6 (*a* and *b*) Fibrous multiscale model results for the 10-$\mu$m-thick case indicate that stresses (*a*) and strains (*b*) propagate throughout the thickness of the substrate. (*c*) The change in degree of orientation from initially random to aligned is greatest at the surface and extends to areas near the lower boundary that are >20 $\mu$m away from the point of deformation at the surface (indicated by the *arrow* in *c*, *inset*). (*d*) The effective stiffness (proportional to peak stress/displacement and normalized to the 50-$\mu$m-thick case) is much greater for the 10- and 30-$\mu$m-thick fibrous models than for nonlinear models with identical loading, geometry, and nonlinear bulk mechanical properties, indicating a greater impact of the rigid boundary in the fibrous model. The simplified model is 75 $\mu$m long and one element in depth (4 $\mu$m), with 2.5 $\mu$m displacement applied over a small area on the top surface as indicated in panel *a*. Due to differences in geometry, results are not directly comparable with the radially symmetric model results in Fig. 4. Scale factors: (*a*) 0–100 Pa von Mises stress; (*b*) 0–0.1 engineering strain; (*c*) 0–1.0 change in degree of fiber alignment. When viewed in greyscale, darker color indicates lower stress in (*a* and *c*), and darker color indicates lower strain in outer areas but higher strain in the central region under the loading in (*b*). Fibrin gel (FG); collagen gel (CG).

relationship than the fibrin gel model, with an 85% increase at 10 $\mu$m and a 20% increase at 30 $\mu$m relative to the 50 $\mu$m model.

## DISCUSSION

In this work, we systematically investigated the distance fibroblasts can feel through fibrous gels by quantifying the spread areas of HLFs and 3T3s as a function of collagen and fibrin gel substrate thickness. The cell areas gradually decreased as gel thickness increased, with the half-maximal spread area of cells on fibrin and collagen gels ($h_{50}$ > 65 $\mu$m) being much larger than published values for PA gels ($h_{50} < 5$ $\mu$m). These results demonstrate that fibroblasts sense much deeper into nonlinear collagen and fibrin gels than they do into linear PA gels. These long sensing distances are consistent with previous observations of surface displacements hundreds of microns from cells cultured on thick fibrin gels (15), strain transfer up to 800 $\mu$m through a collagen gel (26), and increased spreading behavior on soft collagen gels >130 $\mu$m thick (16). Our nonlinear continuum model predicts increases in the effective stiffness that the cell feels only for very low thickness substrates (<5 $\mu$m) indicating that the spreading behavior on thick gels cannot be explained by the strain-stiffening behavior of the material alone. Results from our multiscale model demonstrate substantial changes in effective stiffness at relatively large thicknesses (e.g., 50% greater at 30 $\mu$m than at 50 $\mu$m), suggesting that the fibrous nature of the network enhances depth sensing in collagen and fibrin gels.

In addition to enhancing our understanding of how far cells can sense each other through their extracellular matrix (ECM), the use of rigid boundaries has great potential for creating experimental systems to study the effect of stiffness on cell behavior. For example, Yip and colleagues (2) observed valvular interstitial cell activation to the myofibroblast phenotype (known to be stiffness dependent) on thin collagen films but not on thick collagen gels. Utilizing this approach to modulate the effective stiffness that cells sense has advantages relative to modulating the intrinsic stiffness ECM-based gels (collagen, fibrin, Matrigel, etc.) because it avoids changes in ligand density and presentation that occur when the protein concentration and/or cross-linking are altered. However, for this approach, one must obtain reliable estimates of the effective stiffness as a function of substrate thickness.

### Determining how far cells feel on biopolymer gels

To investigate how far cells can feel through compliant gels, we chose to determine how far into the depth of a gel a cell can sense rather than to analyze lateral cell-cell communication along a substrate, as done previously (27). For high-throughput and self-consistent controls, we utilized variable-thickness gels instead of attempting to control the thickness of individual gels; based on our simulations, the gradient in effective stiffness on these gels is minimal due to the low slope (see Supporting Material). Collagen and fibrin gels are used as model strain-stiffening materials with different fiber structures and degrees of nonlinearity.

In contrast to the rapid decrease in area of cells cultured on progressively thicker PA gels up to a few microns reported in the literature (8,9), our data demonstrate that the rate at which the cell area decreases with increasing thickness of the protein gels is very gradual. Quantitatively, the characteristic sensing distance, $h_{50}$, is >10-fold larger for protein gels than previously reported for PA gels. The relatively small cells from the immortalized 3T3 line

responded almost identically to the primary HLFs, with curves overlapping when normalized to the spread area of control cells on glass (normalized graph not shown). The simple rational equation (Eq. 1) fits the published data very well ($r^2 > 0.9$) and our data relatively well ($r^2 = 0.61–0.77$) without overparameterization. We attribute the lower correlation values for biopolymer systems to the heterogeneity of fiber polymerization, rather than to the choice of regression model. Exact values of $h_{50}$ should be interpreted cautiously, however, because the minimum spread area is not generally reached in published data (9) or in our experimental groups due to limits on confocal working distance (~150 $\mu$m). Despite these limitations, it is clearly evident that cells are able to sense rigid boundaries much farther into collagen and fibrin gels than into linear PA gels.

Current analytical and computational models of cells on gels (including our nonlinear continuum model) predict a decrease in surface displacement with thickness for a given surface traction (7,9,22). The most pronounced changes are predicted on substrates <5 $\mu$m thick regardless of substrate stiffness (28), which is consistent with an increase in effective stiffness and observed cell area (8–10). These models do not predict the more gradual change in cell area in the 5- to 30-$\mu$m thickness range observed on PA gels or the very gradual change in cell area in the 20-150 μm thickness range on protein gels observed in this study.

## Testing the hypothesis that long sensing distances are due to strain stiffening

It is difficult to experimentally separate material nonlinearity from the fibrous nature of the protein gel network; therefore, we computationally investigated the effect of strain stiffening on cell mechanosensing. We used FE models of different material properties and thicknesses to compute the maximum surface displacement that results from a given traction field. From the many metrics for quantifying the distance into a substrate a cell can feel (see Maloney et al. (9) for a tabulated list), we chose to utilize the critical thickness $h_{crit}$, which is analogous to $h_{50}$ in our analysis of measured cell-spreading data. The value for linear gels of 2.41 $\mu$m is in the range of previously reported values from other linear models ($h_{crit}$ ~1.3–3.3 $\mu$m) (7). For the nonlinear gel, the characteristic sensing distance is 35% greater ($h_{crit}$ ~3.3 $\mu$m) due to greater propagation of strain, and it decreases slightly with traction applied (Table 2); however, the critical sensing distance is still far lower than observed for protein gels experimentally. Analysis of the effective stiffness from the nonlinear FE model (Fig. 5, *B* and *C*) also indicates that strain-stiffening behavior representative of a fibrin gel has little effect on the resistance to deformation that the cell senses at the surface for gels greater than a few microns thick.

The material model we utilized in our continuum model simulations was based on available shear stress-strain data from Wen and Jamney (17) for 2 mg/ml fibrin gels. Instead of simulating different polymer concentrations in our model to determine the effect of nonlinearity, we simulated different materials (e.g., collagen) by altering the degree of strain stiffening with a shift to higher transition strain (29). These simulations predict an increase in the magnitude of $u_{max}$, shifting the response from one that is similar to a 2 kPa linear gel to one that is similar to a 1 kPa linear gel, but with virtually no change in sensitively to thickness (Fig. S4 *C*). Higher protein concentration increases the gel stiffness, which would decrease the magnitude of $u_{max}$ but would not be expected to alter the value of $h_{crit}$. The minimal change in $h_{crit}$ for the model with altered nonlinearity is consistent with recent analyses by Hart and colleagues (30). Their FE models of cell interactions on strain-hardening (stiffening) substrates indicate that the propagation of stresses through the substrate is not increased when the parameters of various nonlinear material models are varied over a very large range. Taken together, these results suggest that characteristics other than nonlinearity, such as the fibrous structure, facilitate propagation of mechanical signals through protein gels and result in the observed cell-spreading behavior on relatively thick collagen and fibrin gels.

## Gel fibrous structure likely facilitates long-distance sensing

Due to their high stiffness relative to synthetic PA chains (17), collagen and fibrin fibers are considered as semiflexible filaments or rigid rods with persistence length comparable to fiber length. The lengths range from a few hundred nanometers to micrometers, and are largely determined by the polymerization condition such as pH and ionic strength. Fibrous networks formed through cross-links between fibers (such as in our fibrin gels) or through noncovalent bonds and entanglements (such as in our collagen gels) enhance cell spreading. Winer et al. (15) reported that both fibroblasts and hMSCs spread to a much greater extent on compliant PA gels coated with networks of fibrin compared with gels coated with monomers or filaments of fibrin. We have also observed more pronounced spreading of fibroblasts and heart valve interstitial cells cultured on compliant PA gels when acid-extracted (telopeptide-rich) collagen was utilized as a coating rather than acidic pepsin-extracted collagen, which is less likely to form fibrous networks (A.M. Quinlan and K.L. Billiar, unpublished). Further, given sufficient time, cells cultured on and within protein matrices remodel the protein (15,31,32), which may locally stiffen the protein gel. Thus, the fibrous network at the surface likely explains the relatively large spread area on the soft, thick protein gels, but the existence of surface fibers cannot explain the dependence of cell area on gel thickness in the range of tens to hundreds of microns.

Possible explanations for the long-range propagation of forces and/or displacements include the rod-like structure

of the proteins with high bending stiffness and the interconnected network structure of the fibers. Our analysis of confocal reflectance images indicates that the cells are able to reorganize the surrounding fibrous network structure of both fibrin and collagen gels up to 200 $\mu$m along the surface of the gels. These changes in local reflectance intensity suggest long-range stress and/or strain transfer through the gel, which may extend even farther than we can optically resolve. In 1959, Weiss (33) observed long-range fiber reorganization between groups of cells in fibrin gels, and Stopak and Harris (34) demonstrated centimeter-scale fiber tracts between cell explants cultured on collagen gels three decades ago. Similar local densification around cells cultured within collagen gels has been shown to lead to nonuniform compaction with profound effects on the bulk mechanics of the gels (35). In contrast, in our study, local densification was evident in z-stack images only a few microns below the cells. The lack of visual changes in fiber organization in the XY optical cross-sections may be attributed to orientation of the fibers out of the plane of the images, as predicted by the fibrous FE model (Fig. 6 *C*), and/or to insufficient optical resolution.

The results of the fibrous model indicate that the principal fiber directions extend from the displaced region representing the cell toward the rigid lower boundary at a diagonal (Fig. 6 *C*). The model also predicts substantial changes in fiber orientation $>20$ $\mu$m into the depth of the gel (Fig. 6 *C*, *inset*). In contrast, our linear and nonlinear models indicate that stresses decay to $<10\%$ of maximum values by $<8$ $\mu$m (Table S2), and previous models predict that a rigid surface under an elastic substrate several micrometers or more thick would be undetectable by adherent cells (22). The extensive fiber reorganization in the fibrous model may explain the large change in effective stiffness as gel thickness decreases below 50 $\mu$m that is not evident in the nonlinear continuum model (Fig. 6 *D*). The multiscale modeling approach is a powerful tool for analyzing the propagation of cell-generated mechanical signals through fiber networks. In future studies, fiber parameters such as length, stiffness, and distance between network interconnections can be investigated computationally to determine the effect on stress propagation.

In light of the differences in nonlinear behavior (29) and fibrous network structure of collagen and fibrin gels, the characteristic sensing depths are surprisingly similar for these two protein systems. Collagen and fibrin gels differ in their fiber diameter, fiber length, and architecture. At comparable protein concentrations, the collagen fibrils are found to have larger diameter and greater lengths than the fibrin fibers (32). The fibers in collagen gels are held together through physical entanglements, in contrast to the fibrin fibers, which are covalently bonded together to form a strong elastic network. To determine the key physical properties that govern the distance that cells sense in the fibrous matrix, there is a need to systematically control fiber parameters that are known to alter strain transmission, including fiber diameter, fiber length, and cross-linking density, by varying the polymerization conditions (36).

## CONCLUSIONS

The data from this study demonstrate that cell-induced mechanical signals can transmit hundreds of microns within collagen and fibrin gels and feedback on cell behavior. The continuum FE analyses indicate that the strain-stiffening property of the protein gels is not sufficient to explain the observed behavior. Multiscale models with simplified geometry indicate that fiber realignment plays a large role in stress transfer through the matrix, and the development of models with fibrous elements of various geometry and properties will enable us to further investigate potential mechanisms of stress and strain transfer within protein gels and native ECM. Future experimental work is also needed to determine the effect of fiber parameters, including fiber diameter, fiber length, and cross-linking density, on distance sensing in protein gels. With this knowledge, we will be able to use thin fibrous gels as experimental test beds in which to study cell differentiation, signaling, and other stiffness-dependent biological processes in a native ECM environment. The results of this study shed light on the role of matrix mechanics in regulating cell-cell communication, which is fundamental to understanding wound healing, angiogenesis, and the organization of connective tissues in general. These topics are of critical relevance to tissue engineering and developmental biology.

## SUPPORTING MATERIAL

Supporting analysis, 11 figures, and 2 tables are available at http://www.biophysj.org/biophysj/supplemental/S0006-3495(13)00615-2.

The authors thank Professor George Pins for gracious cell donation and helpful conversations.

This work was supported in part by a grant from the National Institutes of Health (1R15HL087257-01A2 to K.B.) and a National Science Foundation IGERT Fellowship (NSF DGE 1144804 to H.C.).

## REFERENCES

1. Saha, K., A. J. Keung, …, K. E. Healy. 2008. Substrate modulus directs neural stem cell behavior. *Biophys. J.* 95:4426–4438.
2. Yip, C. Y., J. H. Chen, …, C. A. Simmons. 2009. Calcification by valve interstitial cells is regulated by the stiffness of the extracellular matrix. *Arterioscler. Thromb. Vasc. Biol.* 29:936–942.
3. Wang, H. B., M. Dembo, and Y. L. Wang. 2000. Substrate flexibility regulates growth and apoptosis of normal but not transformed cells. *Am. J. Physiol. Cell Physiol.* 279:C1345–C1350.
4. Ingber, D. E. 2003. Mechanobiology and diseases of mechanotransduction. *Ann. Med.* 35:564–577.
5. Vogel, V., and M. Sheetz. 2006. Local force and geometry sensing regulate cell functions. *Nat. Rev. Mol. Cell Biol.* 7:265–275.

6. Discher, D. E., P. Janmey, and Y. L. Wang. 2005. Tissue cells feel and respond to the stiffness of their substrate. *Science.* 310:1139–1143.
7. Sen, S., A. J. Engler, and D. E. Discher. 2009. Matrix strains induced by cells: Computing how far cells can feel. *Cell Mol Bioeng.* 2:39–48.
8. Buxboim, A., K. Rajagopal, …, D. E. Discher. 2010. How deeply cells feel: methods for thin gels. *J. Phys. Condens. Matter.* 22:194116.
9. Maloney, J. M., E. B. Walton, …, K. J. Van Vliet. 2008. Influence of finite thickness and stiffness on cellular adhesion-induced deformation of compliant substrata. *Phys. Rev. E Stat. Nonlin. Soft Matter Phys.* 78:041923.
10. Engler, A. J., S. Sen, …, D. E. Discher. 2006. Matrix elasticity directs stem cell lineage specification. *Cell.* 126:677–689.
11. Engler, A., L. Bacakova, …, D. Discher. 2004. Substrate compliance versus ligand density in cell on gel responses. *Biophys. J.* 86:617–628.
12. Tee, S. Y., J. Fu, …, P. A. Janmey. 2011. Cell shape and substrate rigidity both regulate cell stiffness. *Biophys. J.* 100:L25–L27.
13. Engler, A. J., L. Richert, …, D. E. Discher. 2004. Surface probe measurements of the elasticity of sectioned tissue, thin gels and polyelectrolyte multilayer films: Correlations between substrate stiffness and cell adhesion. *Surf. Sci.* 570:142–154.
14. Reinhart-King, C. A. 2011. How matrix properties control the self-assembly and maintenance of tissues. *Ann. Biomed. Eng.* 39:1849–1856.
15. Winer, J. P., S. Oake, and P. A. Janmey. 2009. Non-linear elasticity of extracellular matrices enables contractile cells to communicate local position and orientation. *PLoS ONE.* 4:e6382.
16. Leong, W. S., C. Y. Tay, …, L. P. Tan. 2010. Thickness sensing of hMSCs on collagen gel directs stem cell fate. *Biochem. Biophys. Res. Commun.* 401:287–292.
17. Wen, Q., and P. A. Janmey. 2011. Polymer physics of the cytoskeleton. *Curr. Opin. Solid State Mater. Sci.* 15:177–182.
18. Knapp, D. M., V. H. Barocas, …, R. T. Tranquillo. 1997. Rheology of reconstituted type I collagen gel in confined compression. *J. Rheol.* 41:971–993.
19. Cameron, A. R., J. E. Frith, and J. J. Cooper-White. 2011. The influence of substrate creep on mesenchymal stem cell behaviour and phenotype. *Biomaterials.* 32:5979–5993.
20. Pelham, Jr., R. J., and Yl. Wang. 1997. Cell locomotion and focal adhesions are regulated by substrate flexibility. *Proc. Natl. Acad. Sci. USA.* 94:13661–13665.
21. Balestrini, J. L., J. K. Skorinko, …, K. L. Billiar. 2010. Applying controlled non-uniform deformation for in vitro studies of cell mechanobiology. *Biomech. Model. Mechanobiol.* 9:329–344.
22. Mehrotra, S., S. C. Hunley, …, C. Chan. 2010. Cell adhesive behavior on thin polyelectrolyte multilayers: cells attempt to achieve homeostasis of its adhesion energy. *Langmuir.* 26:12794–12802.
23. Munevar, S., Y. Wang, and M. Dembo. 2001. Traction force microscopy of migrating normal and H-ras transformed 3T3 fibroblasts. *Biophys. J.* 80:1744–1757.
24. Stylianopoulos, T., and V. H. Barocas. 2007. Volume-averaging theory for the study of the mechanics of collagen networks. *Comput. Methods Appl. Mech. Eng.* 196:2981–2990.
25. Sander, E. A., T. Stylianopoulos, …, V. H. Barocas. 2009. Image-based multiscale modeling predicts tissue-level and network-level fiber reorganization in stretched cell-compacted collagen gels. *Proc. Natl. Acad. Sci. USA.* 106:17675–17680.
26. Vanni, S., B. C. Lagerholm, …, F. Lanni. 2003. Internet-based image analysis quantifies contractile behavior of individual fibroblasts inside model tissue. *Biophys. J.* 84:2715–2727.
27. Reinhart-King, C. A., M. Dembo, and D. A. Hammer. 2008. Cell-cell mechanical communication through compliant substrates. *Biophys. J.* 95:6044–6051.
28. Krishnan, R., B. Oommen, …, K. J. Van Vliet. 2008. Modeling and simulation of chemomechanics at the cell-matrix interface. *Cell Adhes. Migr.* 2:83–94.
29. Storm, C., J. J. Pastore, …, P. A. Janmey. 2005. Nonlinear elasticity in biological gels. *Nature.* 435:191–194.
30. Ma, X., M. E. Schickel, …, R. T. Hart. 2013. Fibers in the extracellular matrix enable long-range stress transmission between cells. *Biophys. J.* 104:1410–1418.
31. Harris, A. K., P. Wild, and D. Stopak. 1980. Silicone rubber substrata: a new wrinkle in the study of cell locomotion. *Science.* 208:177–179.
32. Pedersen, J. A., and M. A. Swartz. 2005. Mechanobiology in the third dimension. *Ann. Biomed. Eng.* 33:1469–1490.
33. Weiss, P. 1959. Cellular dynamics. *Rev. Mod. Phys.* 31:11.
34. Stopak, D., and A. K. Harris. 1982. Connective tissue morphogenesis by fibroblast traction. I. Tissue culture observations. *Dev. Biol.* 90:383–398.
35. Evans, M. C., and V. H. Barocas. 2009. The modulus of fibroblast-populated collagen gels is not determined by final collagen and cell concentration: Experiments and an inclusion-based model. *J. Biomech. Eng.* 131:101014.
36. Roeder, B. A., K. Kokini, and S. L. Voytik-Harbin. 2009. Fibril microstructure affects strain transmission within collagen extracellular matrices. *J. Biomech. Eng.* 131:031004.

# Nonlinear Strain Stiffening is Not Sufficient to Explain How Far Cells Can feel on Fibrous Protein Gels

Mathilda S. Rudnicki, Heather A. Cirka, Maziar Aghvami, Edward A. Sander, Qi Wen,

and Kristen L. Billiar

# Supporting Material

## *Analysis of fiber reorganization in confocal reflectance images*

### Non-uniform intensity profiles along the gel surface

The distance a cell reorganizes the fibers along the surface of a gel was determined by analyzing intensity profiles using ImageJ. Average grayscale values were plotted against distance for 100 pixel-wide regions (as shown by red rectangles in Fig. S1 *A*) fit to polynomial curves. The distance from the cell edge where the grayscale value was indistinguishable from noise (as determined by the intersection of baseline value curve with the data curve), is interpreted as the location where the cell tractions no longer visibly reorganize the matrix. Example average intensity profiles are shown in Fig. S1.

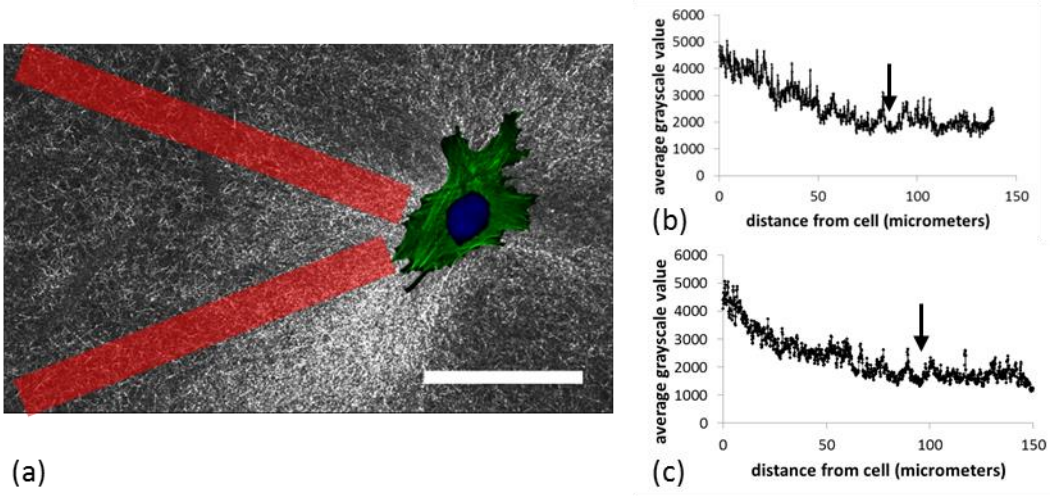


**Fig. S1** (a) Representative confocal reflectance image of a collagen gel (stitched from multiple images) overlaid with confocal image of fluorescently stained cell and example regions of analysis in red. (b and c) Examples of average grayscale verses distance plots for 100 pixel-wide regions of a confocal reflectance image; arrows indicate extent of fiber reorganization from edge of cell located. (Scale bar = 75 μm).

### Skewing of intensity distribution below cells

In our analysis of how deeply into the gel cells affect the fibrous structure, normal probability plots were used to determine the normality of grayscale intensity values in a region of interest of confocal reflectance images. The normal probability plot is a graphical technique used to determine the extent to which a data distribution is Gaussian. In this method, the probability versus error data are plotted (where error in this case is the difference from the average intensity) and the degree to which the plot follows a straight line indicates how well the data can be represented by a Gaussian distribution. Far from a cell and in acellular gels (Fig. S2 *A*), we empirically found that the normal probability plot was linear for ~80% of the data (see Fig. S2 *B*). When the cell remodels the matrix, it creates fiber densifications which skew the

grayscale values in the region of interest towards higher values (Fig. S2 *C*), creating a non-normal distribution (Fig. S2 *D*).

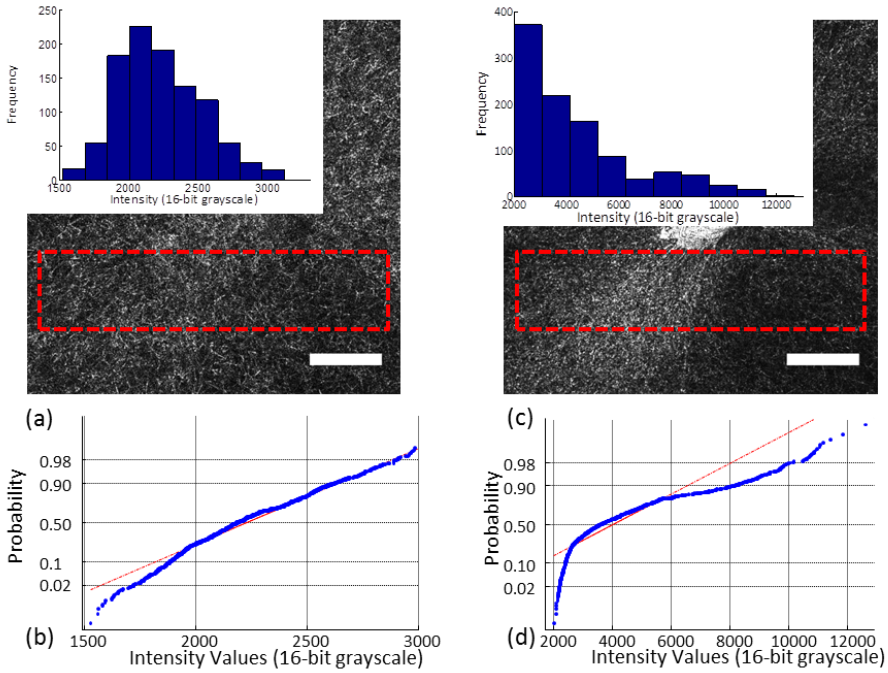


**Fig. S2** Confocal reflectance mode images of 4 mg/ml collagen gel 7.5 μm below cell (a) and at the surface (b). Histograms of intensity (16-bit grayscale) verses distance are shown (insets) for regions of analysis indicated by red rectangles. Probability plots in (c) and (d) correspond to analysis regions in (a) and (b), respectively. Far from the cell, 80% of the data fall along a line indicating a roughly Gaussian distribution of intensities and no measurable effects of the cell on the fiber reflectance pattern (as shown in (b)), whereas cell reorganization of the fibrous matrix at the surface skews the intensity distribution and yielding non-normally distributed data (as shown in (d)).

## *Details on the development of the continuum finite element model*

### Validation of linearly elastic model results

A radially-symmetric continuum finite element (FE) model of a cell exerting inward traction on the surface on a finite thickness gel, as shown in Fig. S3 *A* and *B*, was developed based on work by Sen et al.(1), Mehrotra et al. (2), and Munevar et al. (3).

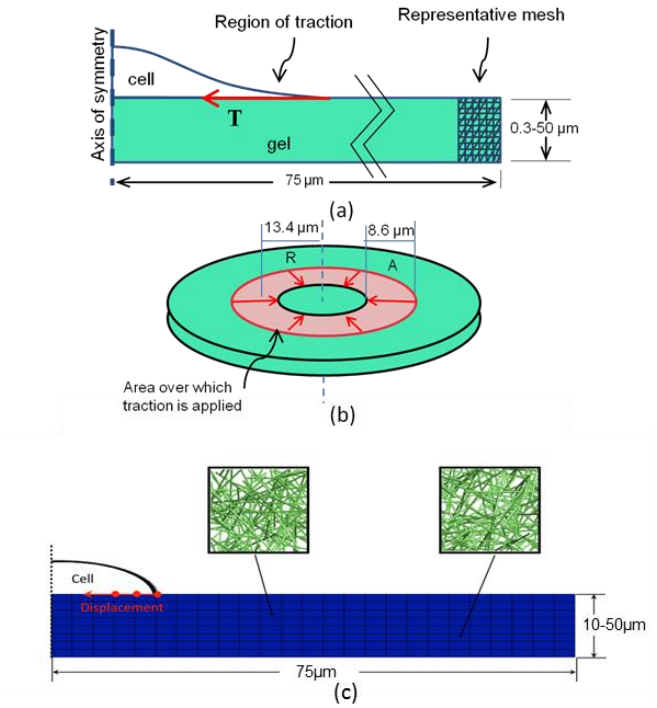


**Fig. S3:** (a) Schematic of the continuum finite element model. Traction is applied to the free top surface of a radially symmetric substrate; the lower boundary is fixed and the left boundary can move only vertically. Nine versions of the model were created in different thicknesses from 0.3-50 µm. The cell is shown for reference but is not modeled. (b) Revolved about the axis, the model simulates a round cell applying traction along an annulus of dimensions provided in the schematic. (c) Schematic of the 10 µm-thick fiber-based finite element model with simplified thin rectangular geometry which is one element deep (4 µm). Displacement is applied to the nodes on the top surface; the lower boundary is fixed, the left boundary can move only vertically, and the front and back surfaces are restrained in the z-direction (into the page). Three versions of the model were created in different thicknesses (10, 30, and 50 µm) with 200 different types of (initially) isotropic fiber distributions (two examples are shown in the figure).

*Degree of strain stiffening of nonlinear material model*

The fibrin gel rheometry data from Winer et al. (4) were fit to a third-order reduced polynomial model in ABAQUS with the following form:

$$W = C_{10}(I_I - 3) + C_{10}(I_I - 3)^2 + C_{10}(I_I - 3)^3 + \frac{1}{D_1} \qquad \text{(S1)}$$

where $W$ is the strain energy per unit volume, $I_I$ is the first strain invariant, and $D_1$ is a compressibility term. The material model was validated by simulating the simple shear experiment using rectangular FE models and comparing the shear stress v. shear strain output with the experimental data (see Fig. S4 *A*).

In an effort to determine the effect of the extent of nonlinearity of the material on substrate displacement, the data from Winer et al. (4) were made "more nonlinear" by increasing the "toe region" of the stress-strain behavior i.e., the strain-stiffening behavior appears at a higher strain as shown in Fig. S4 *B*. The material model has little effect on the normalized displacement-thickness relationship, as shown in Fig. S4 *C*. As the thickness is increased past 20 µm the model becomes unstable and was not used further.

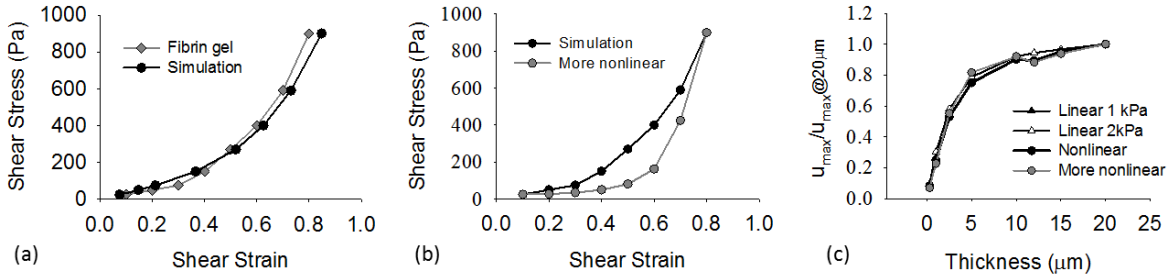


**Fig S4:** (a) The results of the simple shear simulations are compared with the original rheometry data from Winer et al. (12) to ensure that the fibrin gel material responds as intended. (b) The nonlinear material is modified to show stiffening at higher strains. (c) The relationship between substrate thickness and normalized peak displacement values for 1 kPa and 2 kPa linear gels and for the "nonlinear" and "more nonlinear" material models from the FE analysis are qualitatively indistinguishable. Quantitatively, the "nonlinear" material responds similar to the 2 kPa linear gel for thicknesses over 5 μm; the "more nonlinear" material responds much like a 1kPa gel, but the simulations become unstable at h >20 μm and was not used for further simulations.

*Comparison of displacement vs. thickness for the continuum model*

The strain distributions for the linearly elastic model are similar to those published by Sen et al. (1), although the peak strains occur at the inner edge of the applied traction in our model and closer to the cell edge in the previous model. Due to differences in the location of the applied cell traction and definitions of displacement (maximum v. average), our surface displacement v. substrate thickness results are not identical to the published values, yet the results from the two models match closely when normalized to the displacement of the thickest material at each substrate stiffness level. When normalized, the data from each of the four different substrates stiffness levels (E = 1, 5, 12, and 40 kPa) from our model lie roughly on top of those from the previous model (Fig. S5). The normalized displacements from all four stiffness levels of the present model collapse onto a single curve since the system is linear and there is no effect of the cell's stiffness in parallel to the gel.

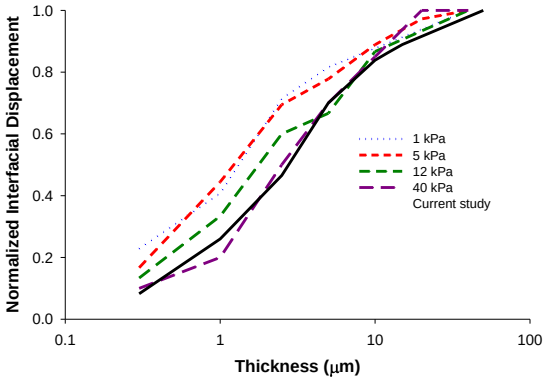


**Fig S5:** Maximum interfacial (surface) displacement predicted from the FE model (in the -x direction) for 500 Pa applied traction as a function of gel thickness, normalized to the value for the "infinitely" thick (50 μm) gel case (solid black line). The normalized displacements from all four stiffness levels of the present model collapse onto the black line since the system is linear. The mean interfacial displacements reported by Discher and colleagues (Figure 4d in Sen et al. (1)), normalized to the value for the "infinitely" thick (50 μm) gel case, are plotted for comparison. Although there are moderate differences in absolute values of reported displacement, the agreement between our model results and those of Sen et al. (1) demonstrates that the functional form of the effect of gel thickness on surface displacement is the same regardless of method of loading (cell prestress v. uniform annulus of traction), radial location of traction, and use of mean v. maximum displacement between our analyses.

**Table S1:** Tabulated data of maximum surface displacement of the FE model for linearly elastic gels of various linear stiffness levels due to 500Pa applied traction

| | **Gel Stiffness (kPa)** | | | |
|---|---|---|---|---|
| **Thickness (μm)** | 1 | 5 | 12 | 40 |
| 0.3 | 0.434 | 0.0869 | 0.0362 | 0.0109 |
| 1 | 1.41 | 0.282 | 0.118 | 0.0353 |
| 2.5 | 2.74 | 0.548 | 0.228 | 0.0685 |
| 5 | 3.79 | 0.758 | 0.316 | 0.0947 |
| 10 | 4.53 | 0.906 | 0.377 | 0.113 |
| 12 | 4.65 | 0.930 | 0.388 | 0.116 |
| 15 | 4.79 | 0.957 | 0.399 | 0.120 |
| 20 | 4.97 | 0.994 | 0.414 | 0.124 |
| 50 | 5.42 | 1.08 | 0.452 | 0.136 |

## Magnitude and location of application of traction

*Changing level of traction*

In terms of the magnitude of applied traction, we chose 50 to 600 Pa (Fig. S6 and Fig. S7) which is in the range of published traction stresses near the edge of a cell and which produces $u_{max}$ values that roughly match measured surface displacements (generally 0.1 to 10 μm). Cell traction forces measured using standard 2D traction force microscopy (TFM) indicate that the traction applied by a cell covers a wide range of values, from up to 250 Pa for human tendon fibroblasts (5) to up to 36 kPa in 3T3 fibroblasts (3) and 430-750 Pa for BAECs (6). Neither our model nor previous models account for the increase in cell traction and spread area with substrate stiffness that is observed in many experimental studies (e.g., 7, 8).

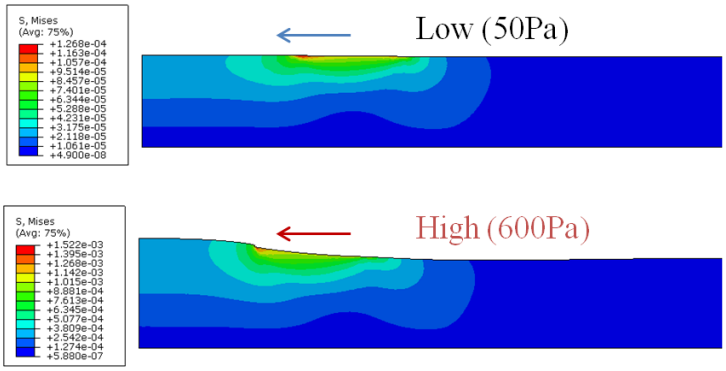


**Fig. S6:** FE stress distribution results of cell-applied traction on 10 μm linear material (1 kPa). Note the similarity of the contour plots, but the difference in material deformation (deformation scale factor=1).

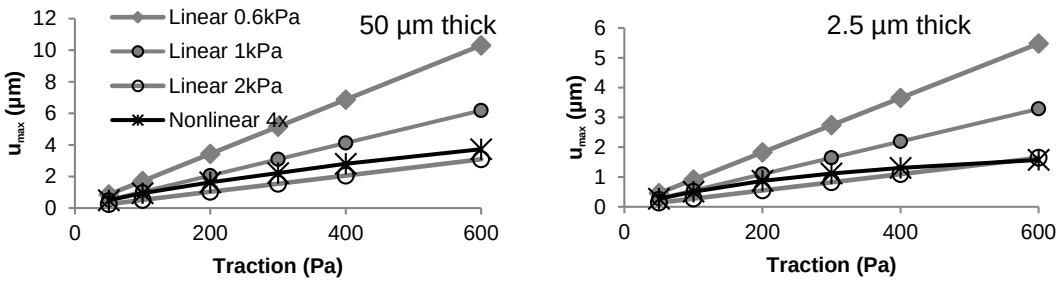


**Fig. S7:** The maximum displacement of the top surface of linear substrates increases linearly as traction is increased. However, the nonlinear material exhibits strain-stiffening behavior; as traction increases, the ability of the nonlinear material to deform is reduced. This strain-stiffening effect is amplified by decreasing the substrate thickness from 50 µm (a) to 2.5 µm (b). On the thin substrate, the gels deform to a lesser extent than the thick gels due to the impact of the rigid boundary under the substrate.

*Changing size and location of cell-applied traction*

The defined area of cell-gel interaction is specified by Mehrotra et al. (2) with two parameters: focal adhesion radius and width of the traction region. When the radius (R) is increased (i.e., a larger cell) or the traction region increases (i.e., more focal adhesions), the maximum surface displacement is increased. Changing the size of the cell or the size of the cell-applied traction surface also affects the effective stiffness of a linear material as shown in Fig. S8 *A*. An increase in R increases the effective stiffness, while an increase in A decreases the effective stiffness. These simulations are performed on a linear elastic substrate to focus on effects of cell geometry.

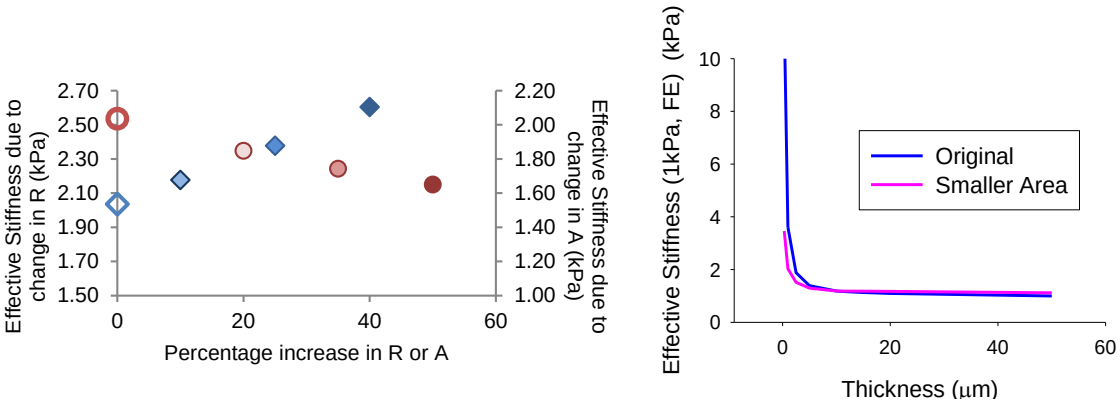


**Fig. S8:** a) The effective stiffness of a linear material is dependent on the dimensions of the applied traction, and thus on the geometry of the cell. Increasing the size of the cell (R, diamonds) increases the effective stiffness of the substrate. Conversely, increasing the size of the traction surface (A, circles) decreases the substrate effective stiffness. b) With the same force but a smaller area for the cell applied traction (traction x area = constant), the linear material responds similarly to the original traction area, in terms of effective stiffness.

The above changes in R and A are performed with a constant traction (100 Pa). Due to the linearity of the material, the value of the applied traction will not affect the overall response of the material. To investigate the effective stiffness response of a cell that applies the same force but only at the very edge of the cell, the model was modified to include a smaller area of cell-applied traction and a higher traction to maintain the same force as 100 Pa over the original area. As shown in Fig. 8 *B*, the effective stiffness of the material with this smaller area follows the same shape as that with the original area.

**Definition of surface displacement: $u_{max}$ vs. $u_{avg}$**

It is not known what physical cues (displacements, forces, strain energy, etc.) a cell senses which causes/allows it to spread more on a stiff surface than compliant one. For a given cell-generated traction, it is reasonable to assume that the resulting surface displacement provides an indication of the stiffness of a surface to the cell, with larger displacement on soft substrates and lower displacements on stiff substrates. Sen et al. (1) utilize the mean interfacial deformation, $u_{avg}$, as a representation of the work done by the cell on the matrix to compare between gel stiffness and thickness levels. In the present study, we utilize the maximum interfacial displacement $u_{max}$, as a metric of the cells' ability to deform the matrix for a given traction, T, applied at a given location, R. We then calculate $E_{eff}$ using these parameters ($u_{max}$, T, R). $u_{max}$ is simpler to extract from the FE output, and is roughly linearly related to $u_{avg}$. To demonstrate this relationship, sample displacement data were collected at nodes along the top of the substrate where traction is applied for the following thicknesses: 0.3, 1, 2.5, 5, 10, 12, 15, 20, and 50 μm, as well as for the following substrate stiffnesses: 1, 5, 12, and 40 kPa. $u_{max}$:$u_{avg}$ = 1.12 +/- 0.01 μm and ranged from 1.05 (on the thinnest gels 0.3 μm) to 1.19 (on a 1 μm thin gel).

**Stiffness gradient**

Using sloped gels allows the simultaneous analysis of many cells' responses to different thickness gels but also creates a gradient in effective stiffness. Strong stiffness gradients (2 and 4 kPa/100 μm) in PA gels have been shown to increase in directional motility and cell orientation relative to non-gradient controls (9). For our study, the slope ($\Delta h/\Delta x$) of the gel was chosen to be as low as practical (~10 μm/mm) with thicknesses ranging from 0 to 300 μm (thickness of a two standard coverslips). When combined with the effective stiffness predictions from the FE model for the nonlinear material with an applied traction of 400 Pa, the gradient in stiffness is 0.02 kPa/100 μm in the 10-50 μm thickness range. Thus our predicted gradient appears to be too low to play a role in the cell response on our substrates.

## *Stress and strain distributions*

Comparison of von Mises stress and strain distribution in linear and nonlinear gels were completed for many thickness levels (1, 10, 50 μm shown in Fig. S9 and Fig. S10, respectively) with traction applied at top surface of 600Pa. All distributions are plotted on undeformed geometry.

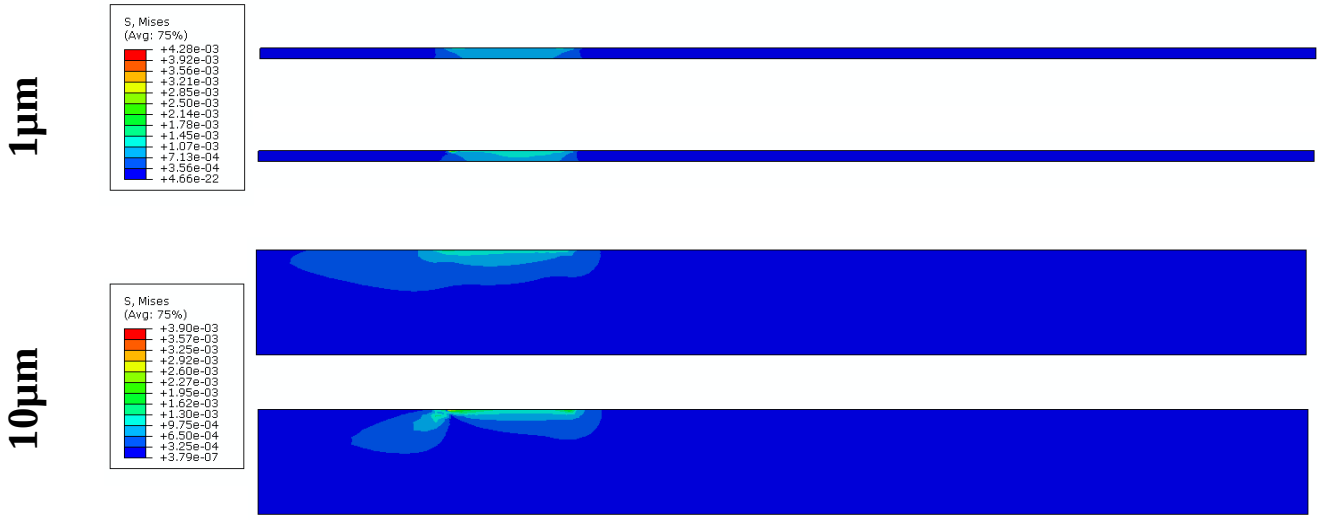

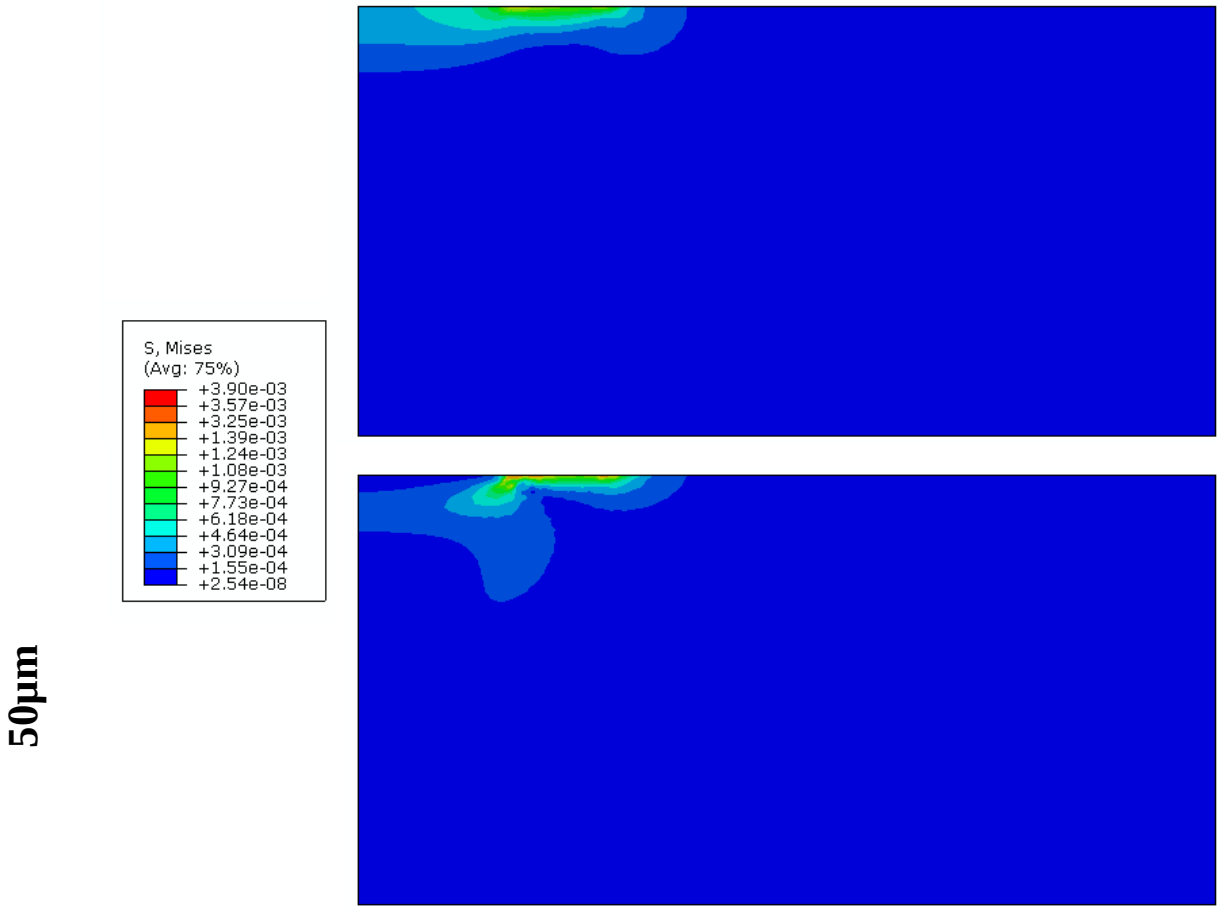


**Fig. S9:** Stress distributions for linear (above, 2kPa) and nonlinear (below, fibrin) gels of 1, 10, and 50 µm thickness, top to bottom with an applied traction of 500 Pa. The color scale is normalized to the maximum and minimum stresses in each case to show the stress profiles regardless of magnitude (deformation scale factor=0). The stress magnitudes for a given thickness are the same regardless of stiffness as expected for linear materials under traction loading (i.e., Boussinesq solution). The stress profiles extend less far into the strain-stiffening material compared to the linear material as can be seen by the distances both laterally and horizontally to the lowest contour, representing roughly 9% of the maximum stress. The stress contours are blunted in the strain-stiffening material.

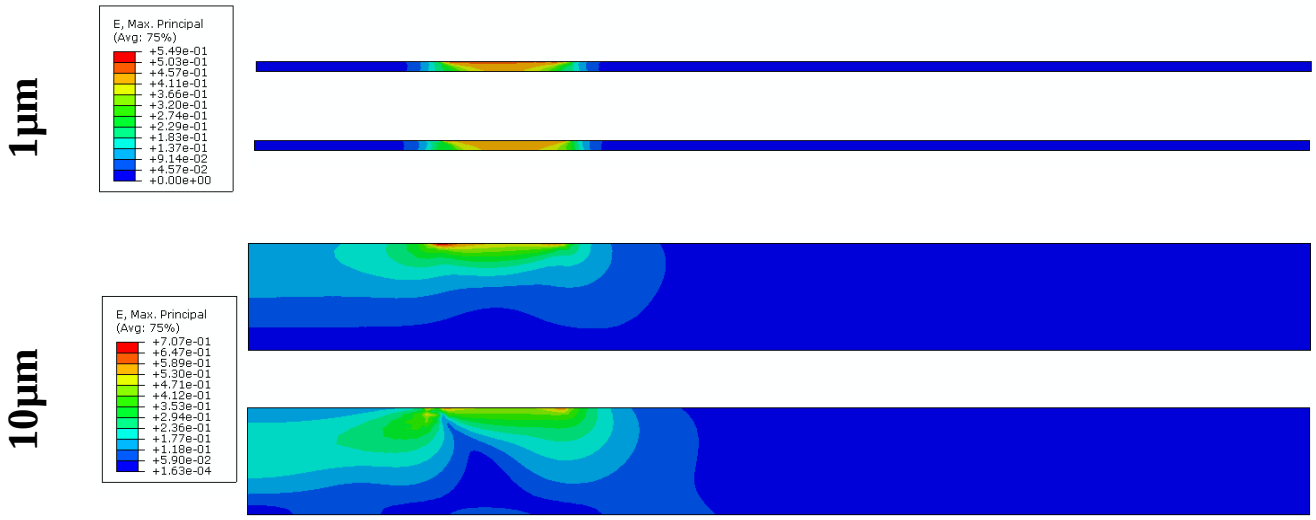

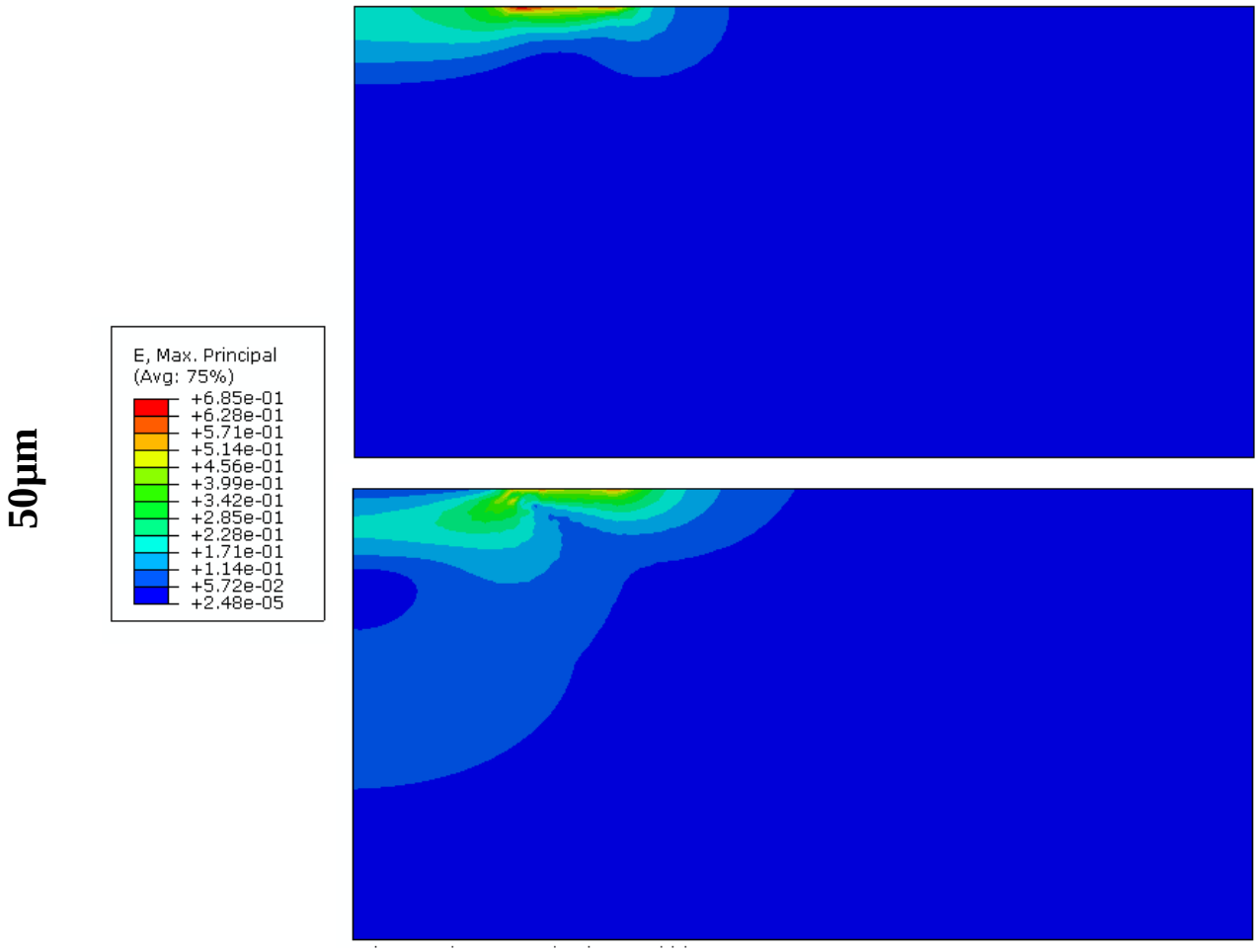


**Fig. S10**: Strain distributions for linear (above, 2kPa) and nonlinear (below, fibrin) gels of 1, 10, and 50 µm thickness, top to bottom with an applied traction of 500 Pa. The color scale is normalized to the maximum and minimum strains in each case to show the strain profiles regardless of magnitude (thus the plots for the other stiffness linear gels (not shown) have different magnitude but look identical). The strain profiles extend further into the strain-stiffening material compared to the linear material as can be seen by the lowest contour, representing roughly 9% of the maximum strain, "touching" the lower boundary in the 10 µm thick nonlinear gel but not in the linear gel.

### Quantitative Comparison of Stress and Strain Distributions

From the above images of stress and strain contour plots of cell-applied traction on linear and nonlinear materials, we see that the stress in the nonlinear material does not travel as far as that in the linear material. In contrast, strains are transmitted further through the nonlinear than in the linear material.

For a quantitative comparison, two distances on the undeformed contour plots were measured for materials of "infinite" thickness (50 µm). The lateral distance from the outer point of the cell-applied traction to the farthest contour line was measured for strain and Von Mises stress for both materials. These variables were also quantified by measuring the vertical distance from the top surface to the farthest contour line along the axis of symmetry. This farthest contour line is the region where the variable is roughly 9% of the local maximum, representing stress or strain that has attenuated to that of the bulk material. The distances are shown in Table S2. Note the larger distance to the farthest strain

contour (strain extending) and the shorter distance to the farthest stress contour (stress blunting) of the nonlinear material compared to the linear material.

**Table S2:** Comparison of distances between the farthest contour line and either the outer edge of cell-applied traction (lateral) or symmetrical axis of the top surface (vertical)

| | | ***Distance to farthest contour (μm)*** | |
|---|---|---|---|
| | | **Linear (1kPa)** | **Nonlinear** |
| **Strain** | *Lateral* | 8.96 | 16.4 |
| | *Vertical* | 8.21 | 37.5 |
| **von Mises stress** | *Lateral* | 8.21 | 6.94 |
| | *Vertical* | 8.21 | 6.88 |

## *Changes in fiber alignment due to surface displacement in multi-scale model*

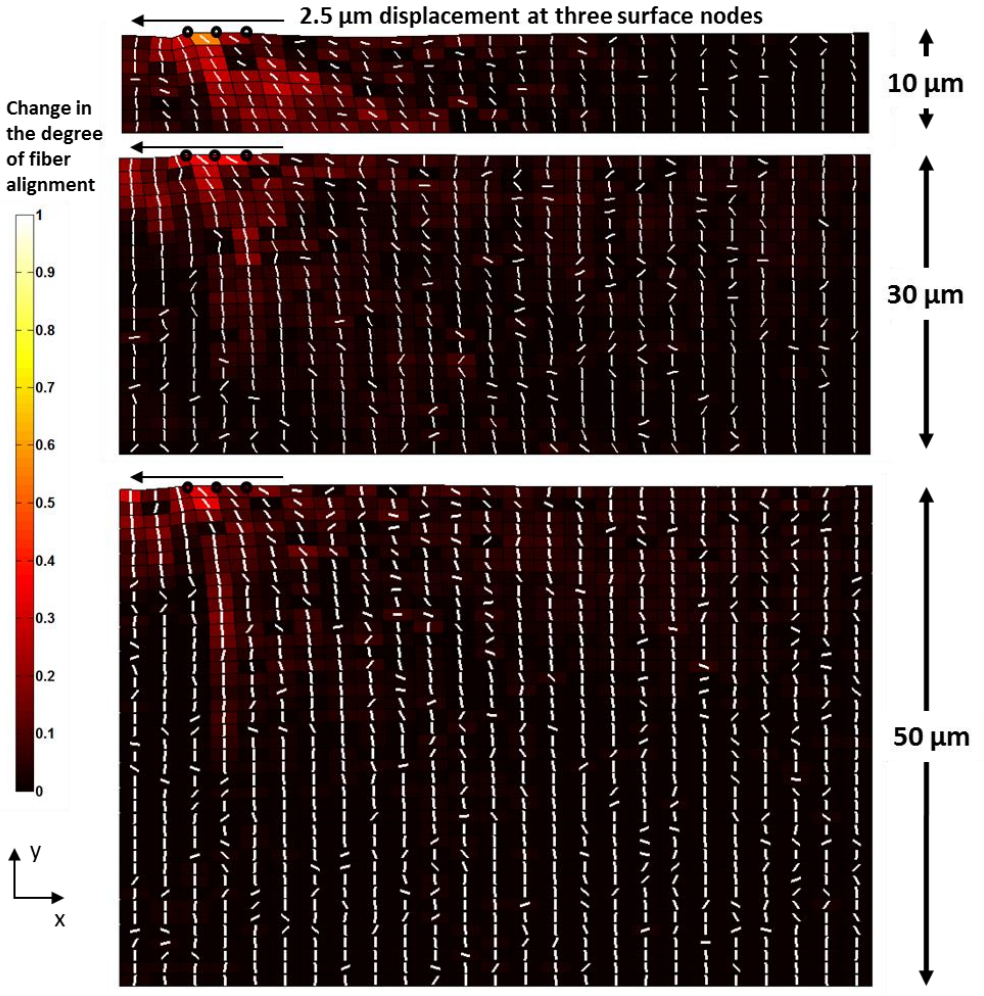


**Fig. S11:** Change in degree of fiber alignment (0-1 color scale) plots for the multi-scale models of 10 μm (top), 30 μm (middle), and 50 μm (bottom) thickness with fiber principal direction quivers (white) superimposed. The surface displacement causes noticeable reorganization of the fiber distributions approximately 15 μm into the 30 μm and 50 μm models, and more than 20 μm into the 10 μm model. The principal fiber directions remain relatively random far from the application of displacement.

## Supporting References

1. Sen, S., A. J. Engler, and D. E. Discher. 2009. Matrix strains induced by cells: Computing how far cells can feel. Cellular and Molecular Bioengineering 2:39-48.
2. Mehrotra, S., S. C. Hunley, K. M. Pawelec, L. Zhang, I. Lee, S. Baek, and C. Chan. 2010. Cell adhesive behavior on thin polyelectrolyte multilayers: Cells attempt to achieve homeostasis of its adhesion energy. Langmuir : the ACS Journal of Surfaces and Colloids 26:12794-12802.
3. Munevar, S., Y. Wang, and M. Dembo. 2001. Traction force microscopy of migrating normal and H-ras transformed 3T3 fibroblasts. Biophysical Journal 80:1744-1757.
4. Winer, J. P., S. Oake, and P. A. Janmey. 2009. Non-linear elasticity of extracellular matrices enables contractile cells to communicate local position and orientation. PloS One 4:e6382.
5. Yang, Z., J. S. Lin, J. Chen, and J. H. Wang. 2006. Determining substrate displacement and cell traction fields--a new approach. Journal of Theoretical Biology 242:607-616.
6. Hur, S. S., Y. Zhao, Y. S. Li, E. Botvinick, and S. Chien. 2009. Live Cells Exert 3-Dimensional Traction Forces on Their Substrata. Cellular and Molecular Bioengineering 2:425-436.
7. Engler, A. J., S. Sen, H. L. Sweeney, and D. E. Discher. 2006. Matrix elasticity directs stem cell lineage specification. Cell 126:677-689.
8. Solon, J., I. Levental, K. Sengupta, P. C. Georges, and P. A. Janmey. 2007. Fibroblast adaptation and stiffness matching to soft elastic substrates. Biophysical Journal 93:4453-4461.
9. Isenberg, B. C., P. A. Dimilla, M. Walker, S. Kim, and J. Y. Wong. 2009. Vascular smooth muscle cell durotaxis depends on substrate stiffness gradient strength. Biophysical Journal 97:1313-1322.